International Journal of Fluid Machinery and Systems DOI: 10.5293/IJFMS.2010.3.3.260
Vol. 3, No. 3, July-September 2010 ISSN (Online): 1882-9554

Original Paper

Study of the Flow in Centrifugal Compressor

Cheng Xu and Ryoichi Samuel Amano

Department of Mechanical Engineering, University of Wisconsin-Milwaukee
Department of Mechanical Engineering, Milwaukee, 53201, USA, amano@uwm.edu

Abstract

Reducing the losses of the tip clearance flow is one of the keys in an unshrouded centrifugal compressor design and development because tip clearances are large in relation to the span of the blades and also centrifugal compressors produce a sufficiently large pressure rise in single stage. This problem is more acute for a low flow high-pressure ratio impeller design. The large tip clearance would cause flow separations, and as a result it would drop both the efficiency and surge margin. Thus a design of a high efficiency and wide operation range low flow coefficient centrifugal compressor is a great challenge. This paper describes a recent development of high efficiency and wide surge margin low flow coefficient centrifugal compressor. A viscous turbomachinery optimal design method developed by the authors for axial flow machine was further extended and used in the centrifugal compressor design. The compressor has three main parts: impeller, a low solidity diffuser and volute. The tip clearance is under a special consideration in this design to allow impeller insensitiveness to the clearance. A patented three-dimensional low solidity diffuser design method is used and applied to this design. The compressor test results demonstrated to be successful to extend the low solidity diffusers to high-pressure ratio compressor. The compressor stage performance showed the total to static efficiency of the compressor being about 85% and stability range over 35%. The test results are in good agreement with the design.

Keywords: centrifugal compressor, flow separation, static efficiency, turbomachinery, impeller, surge.

1. Introduction

The flow enters a compressor axially with the action of the centrifugal force and it turns in the radial direction out from the impeller. The flow then is directed to a radial annular vaned or vaneless diffuser. The flow exit from diffuser needs a volute or collector to deliver the flow to the next stage or send to the next components [1-5]. Unlike an axial compressor or fan [6], the work input for centrifugal compressor is almost independent of the nature of the flow. A centrifugal compressor can be designed with much higher De Haller number than an axial compressor can achieve. Therefore, it is possible for a centrifugal compressor to have a much higher stage pressure ratio than axial ones. Centrifugal compressors have wide applications for a mass flow rate less than 10 kg/s [1-5, 7].

As is well recognized, low flow coefficient centrifugal compressors have wide applications in turbo shaft aircraft engines, petrochemical plants, and manufacturing. However, being in a low-power class, these compressors need to be inexpensive to manufacture and operate, requiring that the compressor having a simple design with less number of parts and a smaller relative tolerance. Moreover, the five-axial machine is now a common tool for impeller machining, but most other parts should be fabricated by using other type of machining to reduce the manufacturing costs.

Turbomachinery industries are interested in using optimization procedures that enable to enhance compressor efficiency and wide operating ranges. Turbo machine design normally starts with a meanline program at each individual operating point on a map, then throughflow calculation is performed, and finally, the impeller, diffuser and volute are designed. In this study, a recently developed turbomachinery viscous optimal method [8,9] especially for axial machines was further extended to a centrifugal compressor design. The main focus of this study lies in a development of a flow coefficient in the order of $\phi = 0.145$ compressor. The design requirements for this compressor development are that the compressor stage pressure ratio is 3.65 and a preferred flow rate is about 0.75 kg/s at the design condition with a total to static efficiency larger than 84% and the stability range SB≥30%. The compressor design employs a viscous process for achieving efficiency and stability targets. Good surge margins were achieved without use of a variable geometry for a steady-state operation. Special attention has been paid to a tip clearance

Received July 27 2010; accepted for publication September 7 2010: Review conducted by Prof. Zhang Yangjun (Paper number O10019C)
Corresponding author: Ryoichi Samuel Amano, Professor, amano@uwm.edu

during the impeller design. The compressor developed in this study consists of three major parts: an impeller, low solidity diffuser, and volute. In this study, particular attention was paid mainly on impeller and low solidity diffuser development.

2. Outline Of The Design Process

The design of modern industrial centrifugal compressors requires the aerodynamic optimization of each component. Typically, the detailed design cycle starts with a parametric study involving the vector diagram by means of a one-dimensional mean-line study. Normally, after the mean-line study, two-dimensional analyses are conducted, which is followed by the designs of impeller, diffuser vane, and volute. The design parts were analyzed by employing a three-dimensional blade-to-blade flow analysis. The volute design is based on the conservation of the momentum and conservation of mass in this study [10]. The attention of the volute design was paid to the tongue shape [11]. After each iteration of the optimization study, the impeller or diffuser performance was estimated. Then, the optimal design of impeller and diffuser were attained based on the design condition, overall computational fluid dynamics (CFD) analysis for each component of the machine was conducted. The stage parameter optimization study was performed before the final stage was designed. This paper focuses the impeller design as well as an incorporation of a diffuser design.

In general, there are three types of design processes for impeller and diffuser blades: inverse, direct and hybrid direct-inverse designs [8,9]. The inverse design is faster because it is based on the two-dimensional flow analysis to form the blade or airfoil according to a pressure profile. However, the location of the profile control points is difficult to control and numbers of arcs are generally large. This makes it difficult to use the same curve definition routine for design and manufacturing. At the same time, direct design may require more time in the aerodynamic design process, but one can generate more accurate designs in the manufacturing process. The hybrid direct-inverse design method is still not mature enough to use in the airfoil design. The present study focuses on the development of the direct design process. The direct design process is to design the blade and airfoil profile by representing the blade and airfoil as curves and to check the performance by a fast computing two-dimensional code [8,9].

After each basic impeller blade and diffuser profile is designed, a fast performance evaluation code is used to check the airfoil performance [8,9]. Then, the impeller or diffuser is designed, a quasi-three dimensional code is developed to more accurately check the airfoil performance in order to judge them whether it needs redesigning or not.

Impeller blade and diffuser airfoil shapes can be represented in different ways. One of them is to represent as curves in the different parts. Because blade and airfoil shape are favored to have a smooth curve to avoid unexpected flow circulation and separation, it requires a second-order continuity property. The Bezier curves have this property of continuity. The Bezier curves may be represented by using control points P_i ($i=0$ to m). Then the curves can be defined parametrically as follows:

$$B(t) = \sum_{i=0}^{m} P_i b_{i,m}(t) \tag{1}$$

where $B(t)$ is a point on the curve for the parametric value t and can be represented as

$$B(t) = \begin{bmatrix} x(t) \\ y(t) \end{bmatrix} \tag{2}$$

P_i ($i=1$ to m) is the control point,

$$P_i = \begin{bmatrix} x_i \\ y_i \end{bmatrix} \tag{3}$$

and the Bernstein basis function is

$$b_{i,m}(t) = \frac{m! t^i (1-t)^{m-i}}{i!(m-i)!} \tag{4}$$

Numerical optimization techniques are used in different steps for different components of aerodynamic design [12-15]. However, due to a complex three-dimensional nature of flow, Computational Fluid Dynamics (CFD) calculation is still a time consuming process. Most of the optimizations [13] were performed mainly in impeller design. Although optimization of the single component is very important, the overall optimization is more critical.

The optimization design method has been developed in the recent decades for a complex system and its subsystems while observing all design requirements and constraints, objectives and goals. In the mean-line optimization, a design of experimental method was used to optimize the machine efficiency. Recently, a Six Sigma based probabilistic design optimization formulation [16] has been used to optimize the engineering designs. Variability is incorporated within all elements of probabilistic optimization formulation. In the design optimization process, a deterministic optimization is applied first before the resulting design is evaluated for quality by measuring reliability and robustness. The quality of the design is then improved by implementing Six Sigma probabilistic optimization and the resulting tradeoff is evaluated. This method was used in the impeller and diffuser blade design optimization.

It is known that the flow behavior inside any component of compressor stage not only determines the aerodynamic efficiency of that component itself, but also strongly affects the flow of the downstream and upstream components. The flowchart of the design process is shown in Fig. 1. The design procedure includes mean-line analysis and parameter optimization, impeller, diffuser, and volute design and optimization, and CFD analysis and optimization steps.

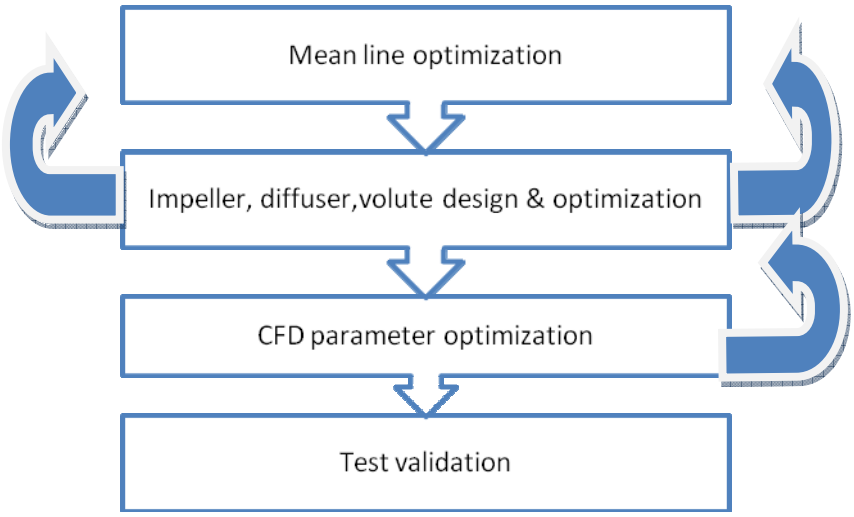

Fig. 1 Centrifugal design process.

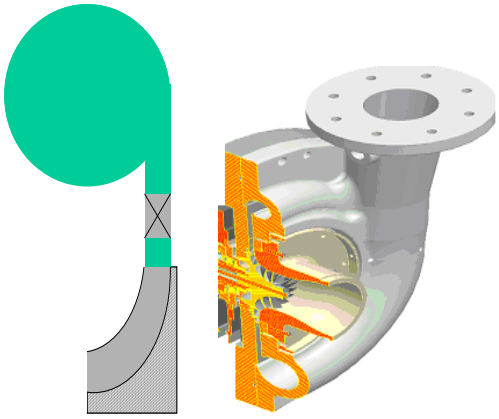

Fig. 2. Cut away view

3. Impeller Design

A centrifugal compressor stage consists of three main components: a rotating impeller, diffusers, and a volute as shown in Fig.2. The low flow coefficient impeller design is critical in terms of aerodynamic efficiency and operating range of the compressor stage. Impeller aerodynamics also impacts the performance of the diffuser and volute. It is very important to achieve an optimized configuration of the impeller. The traditional impeller design has been performed by using a one-dimensional analysis; then, the blade and endwall geometries were selected according to the standard criteria so that the new impeller has a scale of an exiting one. This design method could not provide the predication of the impeller flows in order to improve the design; therefore, the flow separation in the impeller is a necessary consequence of the stipulation of the impeller geometry in most cases.

In this study, one-dimensional studies were initially performed to do parameters studies. It was shown that the rotational speed at design condition of 65,000 rpm was necessary to achieve high compressor efficiency and to maintain overall diameter objectives. Due to the limitations of motor and structure, the design rotational speed was set to 59,000 rpm. The blade tip to hub diameter ratio is about 0.34 and an inlet absolute average Mach number is about 0.4. The inlet relative tip Mach number is about 0.9. The impeller was designed without splitter due to the size of the impeller and manufacturing restrictions. A high impeller backward exit angle was used in this design to improve the efficiency through the reduction of the impeller loading and to improve a surge margin by providing a steeper energy addition characteristic. The high impeller exit blade angles required a coordinated aeromechanical design effort.

The detailed flow structure and impeller performance were analyzed by using the Computational Fluid Dynamic (CFD) analysis to help a parametric study and an optimization. In order to perform the optimization, a number of geometrical parameters were identified. The design modifications were made by varying the values of such parameters. The final impeller was designed by using a fast three-dimensional viscous code [14].

H-type of mesh [14,15], which is suitable for obtaining low-skewed grids around long and thin blades, was employed to compute the flow in a single blade passage. Grid sizes were chosen in order to accomplish a grid independent state to have enough

accuracy and fast enough for design and optimization. After several preliminary studies it was shown that the computational grid size of 43×43×153 was grid-independent; and thus was used for all of the design simulations through this study. The typical meridional mesh is shown in Fig. 3.

The computation was carried out based on the single blade passage during the impeller design. After each calculation was done, a Design of Experiments (DOE) Optimization study was performed [12,13]. For every calculation, the convergence was set when the residual RMS level with at least a fifth order of magnitude reduction with respect to its initial value. The typical convergence history is shown in Fig. 4.

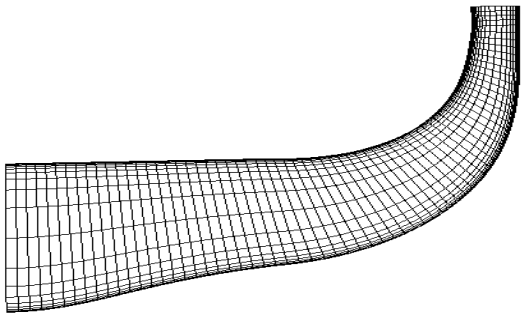

Fig. 3. Mesh in meridional plane.

(Half of the mesh points are made visible)

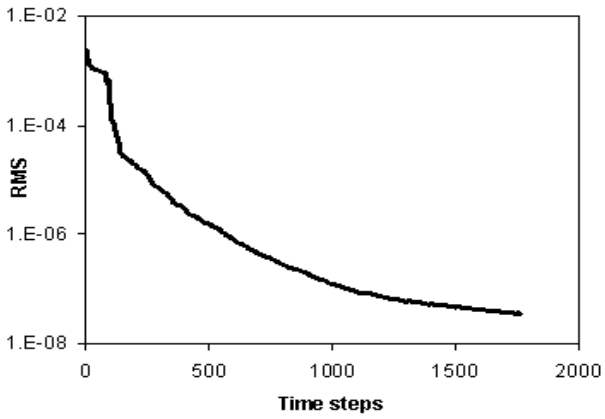

Fig. 4 Convergence history.

With several iterations of optimizations, the final impeller was designed. The meridional channel shape has characteristics at both inlet and exit with a straight channel and middle has relatively large curvature. The impeller hub and shroud relative-velocity distributions at design pressure ratio are shown in Fig. 5. The final blade has a backswept angle $\beta=56^{o}$. The final blade angle distributions at blade hub and shroud are shown in Fig. 6. The final blade angle was adjusted after the optimization study at design point. The impeller blade angle was set to about 3^{o} incidence at both tip and root sections in order to increase the choke margin. The blade angles at both shroud and hub combined with meridional channel shape provide the reasonable blade loading as shown in Fig. 6. The static pressure contour at mid meridional plane between two blades is shown in Fig. 7. The velocity vectors for the flow near the blade pressure-side and suction-side are shown in Figs. 8 and 9, where one can note that the flows are well organized inside the impeller with only the small separation region appearing near the tip of the blade. Fig. 10 shows the relative velocity vectors along the shroud surface near the impeller exit. It is depicted in this figure that a flow separation appears near the shroud tip region. Flow separations were induced by the large tip clearance (2% of the exit width) at the tip due to the blade-trailing wake and pressure gradient. Several efforts were made to eliminate flow separations. The variable tip clearance was used to reduce the separation. The reduction of the shroud loading and reduction of the blade trailing edge thickness showed the improvement of flows near the shroud tip ranges. However, the reduction of the shroud loading increased the hub loading which caused the flow separation at the hub. The reduction of the trailing edge thickness caused the mechanical stress and vibration frequency problems. Due to the limitation of the development time, current design was used as the final design. Variable clearance can reduce the affects of efficiency with the change in the axial tip clearance as shown in Fig. 10. As shown in Fig. 11, the low clearance sensitivity allows the impeller to operate at the clearance up to 6% of clearance to exit blade height ratio without dropping efficiency 3%. The variable tip clearance allows the impeller manufacturing having a relatively large tolerance and also renders impeller operational work in an extremely severe condition such as a fast rapid acceleration like turbocharger and a helicopter engine. The absolute flow angle contours at the rotor exit are shown in Fig. 12. As seen in this figure, only the flow region close to the tip entails a high flow angle. This is because the meridional velocity is very low in this region.

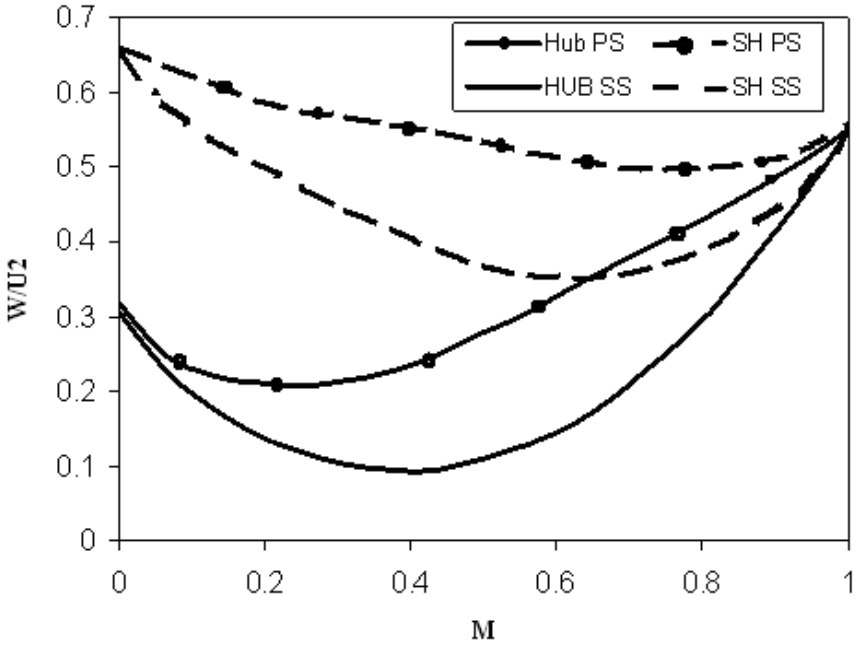

Fig. 5 Blade surface velocity distributions

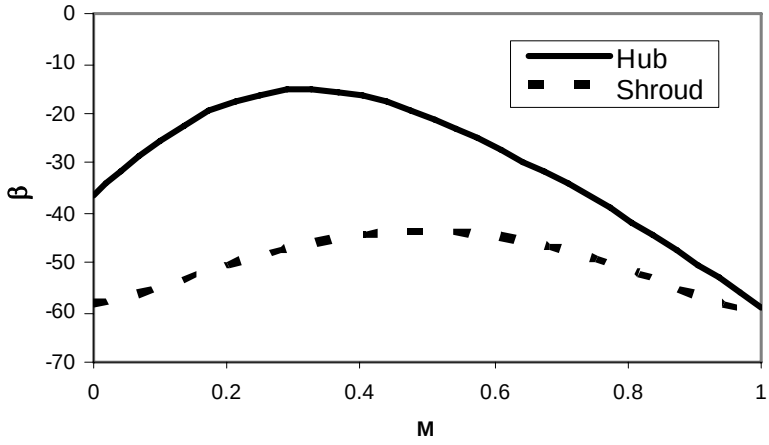

Fig. 6 Blade angle distribution.

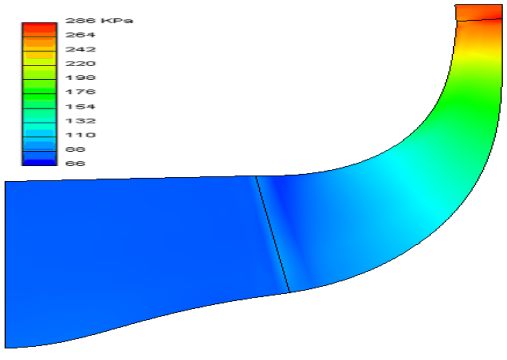

Fig. 7 Static pressure distributions at mid-plane between two blades.

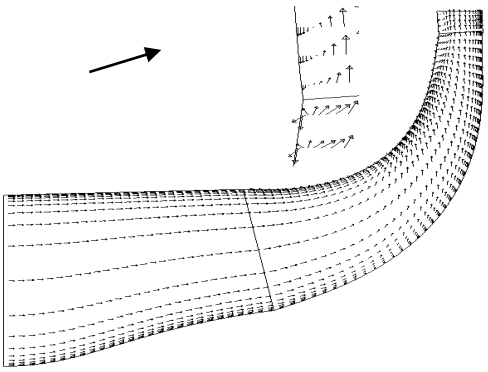

Fig. 8 Velocity vectors near pressure surface.

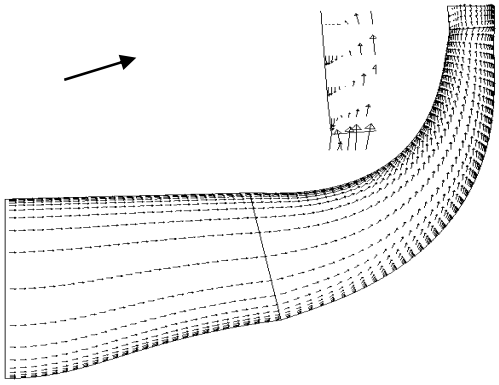

Fig. 9 Velocity vectors near suction surface.

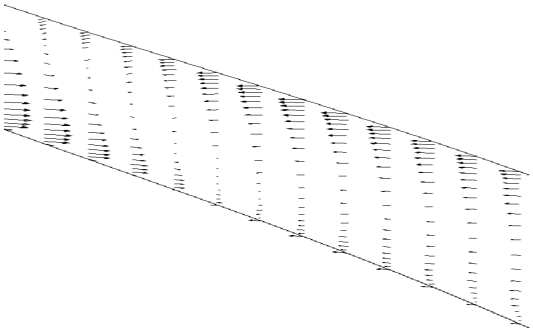

Fig. 10 Relative velocity vectors near shroud surface.

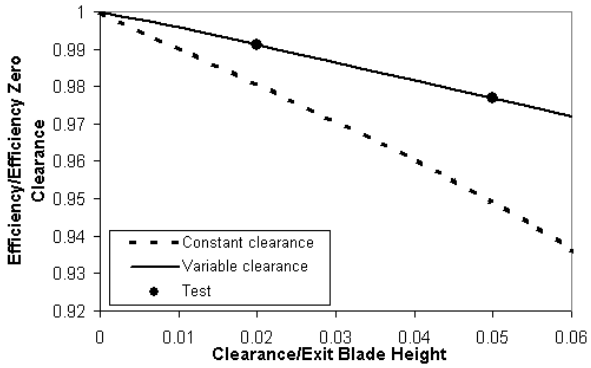

Fig. 11 Tip clearance sensitivity.

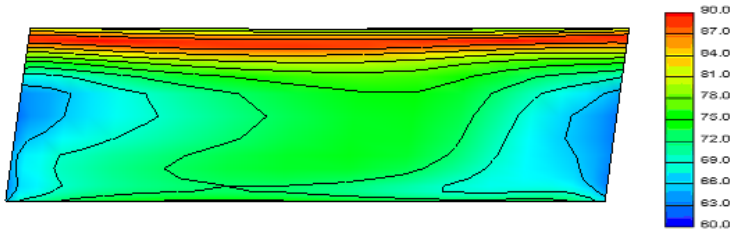

Fig. 12 Absolute flow angle contour at rotor exit.

4. Diffuser Design

A vaned diffuser has become more popular because of its high efficiency feature compared with a vaneless diffuser. However, the problem with a conventional vaned diffuser design compressor lies in the fact that the operating range is often relatively small compared with a vaneless diffuser [2]. In order to overcome this problem, a low solidity vaned diffuser was proposed [2,5,17]. The low solidity diffuser research showed that a low solidity diffuser could provide not only a higher efficiency but also a reasonable operating flow range. As a remedy, different types of vane shape were tried for a low solidity diffuser. However most of the diffuser vane shapes were either derived from a NACA airfoil or just a flat plate [2,5] and the applications of the low solidity vaned diffuser were limited in low pressure ratio machines. In the present study, in order to meet the higher efficiency and wide flow operating range requirements, a diffuser was designed to apply to this high-pressure ratio machine. The diffuser was generated by optimizing sections and stacking them up by using three-dimensional analyses [8,9].

In this part of the designs, the solidity of the diffuser is $\sigma = 0.7$. Given the solidity and inlet conditions, change of the vane number will cause to alter the length of the vane and the turning angle of the vane. The blade loading was thus changed. After the optimization study, the number of the diffuser vanes was set to nine, which gives a high efficiency and a better flow control. Three diffuser vane sections were designed and optimized for each section [9]. The diffuser vane airfoil sections were designed based on the inlet condition of impeller CFD analysis and the exit static pressure condition of the design requirements. After completion of the design of each section, the diffuser blade was stacked-up based on three-dimensional analyses. The final diffuser was obtained after several optimization analyses. The typical mesh of the diffuser analysis at mid-span is shown in Fig. 13. The H-mesh was used and generated by employing different blocks. The design condition at mid-span pressure contour (Fig. 14) shows that there is a little incidence at the diffuser vane. This small incidence allows the compressor to have a wide operating range and have a relatively high efficiency at off-design conditions. The velocity vectors, Fig. 15, show that the flow field is well organized. There is no separation found in the design condition.

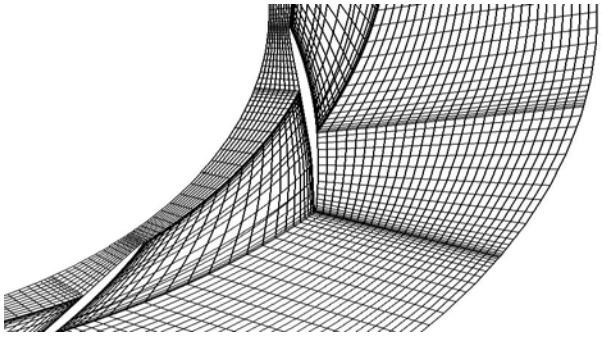

Fig. 13 Mesh at the mid-span of the diffuser.

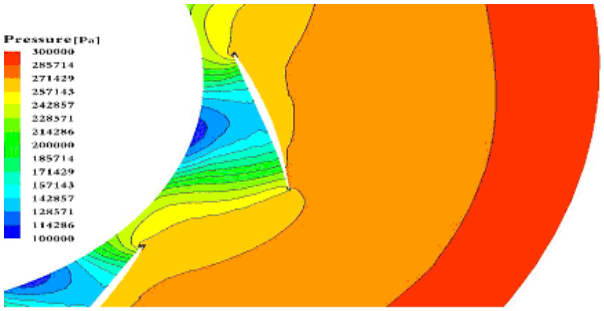

Fig. 14 Static pressure contour at mid-span.

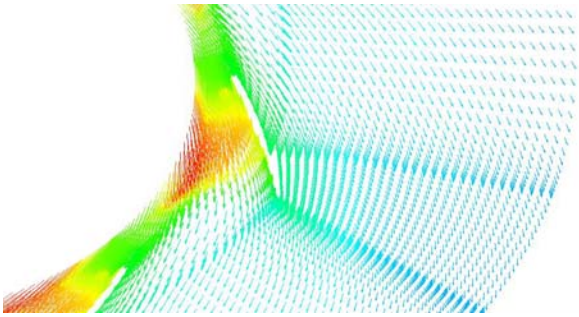

Fig. 15 Velocity vector at mid-span.

5. Performance Prediction and Test

The presently considered compressor was designed by using a viscous design method by optimizing both efficiency and surge margin. In this design, the compressor performance was calculated by using the mean-line calculation and combination of the blockage and loss results from three-dimensional viscous flow analyses. The full compressor stage CFD analyses only run for three points, i.e. near surge, design and near choke conditions. The loss and blockage between three points were obtained using a linear relationship.

In CFD analysis, the structure hexahedral meshes are generated to define inlet pipe (541056 cells), impeller (541056 cells) and diffuser zones (541056 cells), while the unstructured tetrahedral cells are used to define the volute (470,614 cells) as shown in Fig. 16. The impeller stability operating range (SB) was defined from choke to a surge point. The choke point is simulated by reducing the back-pressure with an increasing strength of the shock at either impeller inducer or diffuser vane throat. Stall is an unsteady phenomenon, which is impossible to simulate by using a steady flow analysis. However, the investigation of the stall inception by using the steady code can provide important information of the surge margin. In this analysis, the surge point is defined when the computation is not converged if the flow rate is reduced. The computational results are shown in Fig. 18 for the case of tip clearance of 2%.

The designed compressor stage was built and tested in an open loop test rig (Fig. 17). Air was drawn from ambient and discharged to ambient. The impeller was driven by an electric motor coupled with a gearbox. The test was performed at design impeller rotational speed and two different tip clearance settings were used, i.e. 2% and 5% of blade height. The mass flow rate of the compressor was measured at the discharge by a calibrated ASME nozzle [17]. The flow rate measurement uncertainty was within 2.0% and the speed was measured with a one pulse per revolution signal sensed by a magnetic probe, which looks to be a notch in the shaft. The measurement uncertainty of the speed was less than 0.01%, which has a very insignificant effect on the stage performance measurement. The temperatures were measured by using Type E half-shielded thermocouple. The uncertainty of the temperature measurement is about 0.25%. The measurement uncertainty for total pressure and static pressure are 0.25% and 0.15%, respectively. The inlet upstream and stage exit conditions were measured by employing five Kiel probes and five thermocouples at upstream of three time of impeller inlet pipe and discharge. Ten wall static pressure taps were used for the measurement of the inlet and discharge static pressure. The measurement results for the tip clearance effect are shown in Fig. 11. It is shown that variable tip clearance has a better effect on the rate of efficiency loss with increasing the tip clearance. The performance measurement is shown in Fig. 18. The experimental results show a good agreement with the calculations. Due to the stall phenomena during the test when the compressor is close to the stall, the vibration level increases. For the safety purpose of the bearing system, the test machine did not run to the machine surge. It was shown that except the flow close to choke range, the CFD provided a good estimate of the compressor performance. For the compressor flow close to choke, CFD provided more flow range than performance test.

It is showed that the design analyses and performance predications agree well with tests. The design procedures developed here produce a very competitive design for both peak efficiency and operating range. It is shown that the centrifugal compressor design procedure developed by this research provided a fairly successful design.

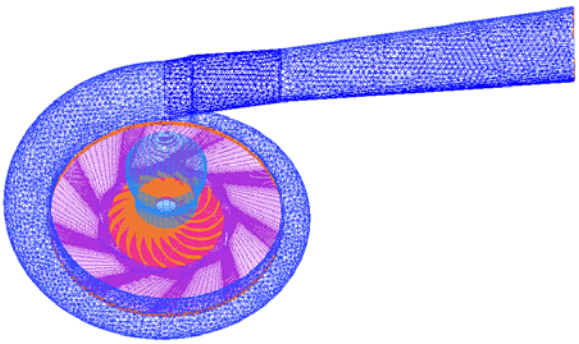

Fig. 16 The computational mesh for compressor.

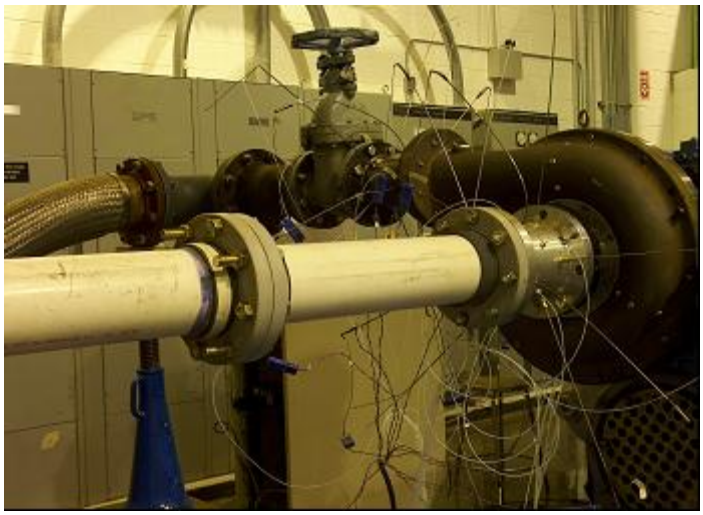

Fig. 17 Test rig of a single stage compressor

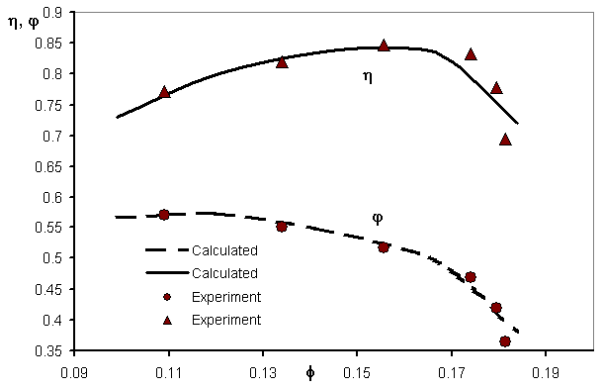

Fig. 18 Compressor performance.

5.1 Volute

Fig. 19 shows the static pressure distribution at mid span of the volute and diffuser. It can be seen that, for all the flow cases, the static pressure distributions near the vane diffuser inlet are symmetric and static pressures near volute inlet are distorted. The flow near choke presented the highest static pressure distortion at the inlet of the volute. The unsymmetrical pressure distributions inside the diffuser also cause the variations of the Mach number as shown in Fig. 20. The isentropic Mach number distributions show that, by increasing the compressor flow rate, the highest Mach number location moves downstream from vaneless diffuser to vaned diffusers. When the flow rate approaches closer to choke, the position of the highest Mach number moves toward the leading edge of the diffuser vanes. The diffuser vane inlet throat limited the maximum compressor flow, which causes a flow choke.

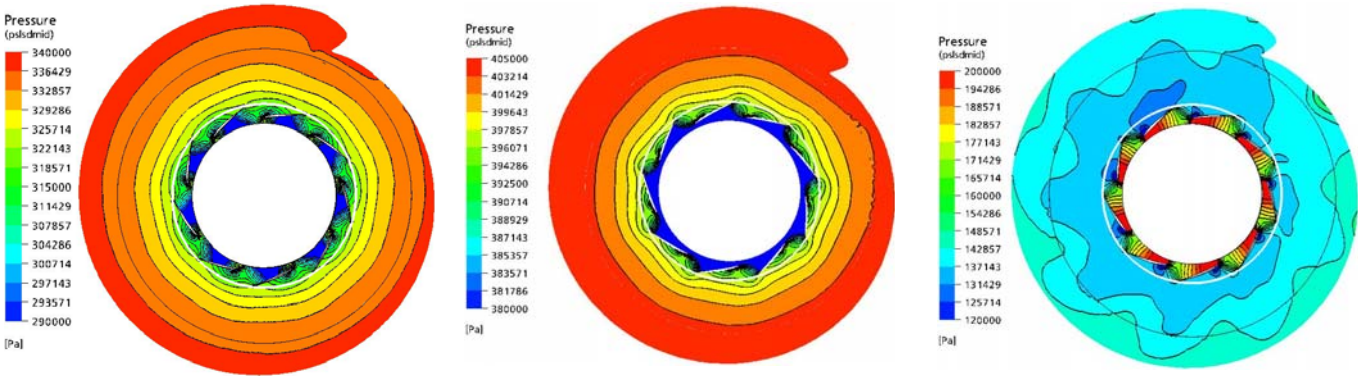

a. ϕ/ϕ_0 =1.08 b. ϕ/ϕ_0=0.7 c. ϕ/ϕ_0=1.25

Fig. 19 Static pressure contours at mid-span.

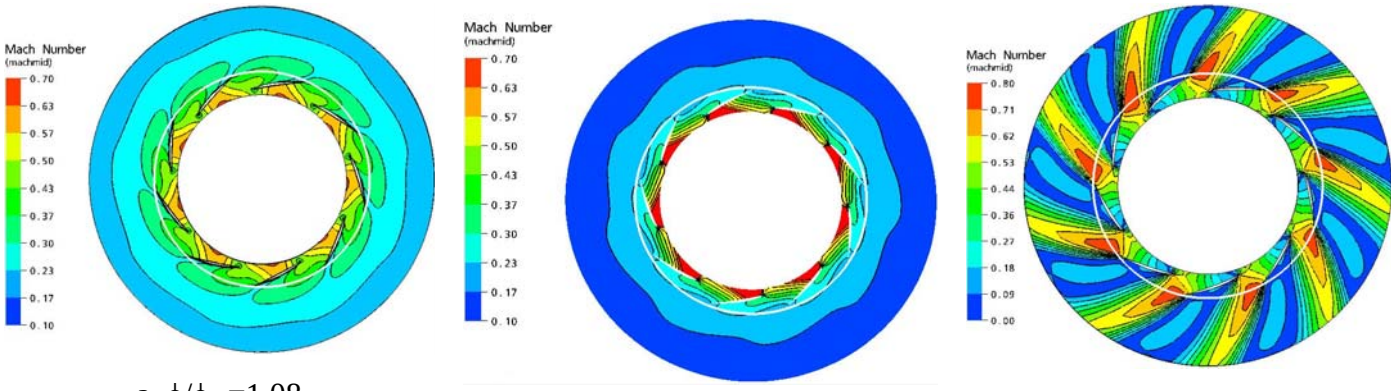

a. ϕ/ϕ_0 =1.08 b. ϕ/ϕ_0=0.7 c. ϕ/ϕ_0=1.25

Fig. 20 Mach number contours at mid-span.

6. Conclusions

A low flow coefficient high-pressure ratio single stage centrifugal compressor was designed by using a viscous optimization method. This compressor is capable of a high performance. A wide operating range was achieved without resorting to variable geometry and flow controls. The experimental results showed that the design is in good agreement with the test results. The applications of CFD provide the reliable design. It is proven that the design system developed in this study is feasible; the design thus provides a useful tool for a future centrifugal compressor development. The future development for this machine will be focused on the three-dimensional optimization of the impeller, and will introduce better material in order to build the impeller blades thinner and flow control investigation of impeller tip region.

Nomenclature

b = Bernstein basis function	PR_d = pressure ratio at design point
C = absolute velocity at impeller outlet	Q = volumetric flow
D = diameter of impeller	SB = (Q_c-Q_s)/Q_c
i = point number	SM = (PR_s-PR_d)/PR_d
L= chord length	t = parameter
M = non-dimensional meridional curve length	U = peripheral velocity
N = impeller rotation speed (rad/s)	W = relative velocity
p = diffuser leading edge pitch = $2\pi r_3/Z$	x, y = coordinates
P = control point	Z = number of vane or impeller blade
PR_s = pressure ratio at surge	

Subscripts

1 = impeller inlet	s =surge point
2 = impeller exit	o = operation point
3 = diffuser inlet	p = polytropic
c = choke point	r =radial direction
d = design point	

Greeks

β = blade angle from radial direction	σ = solidity (= *L/p*)
ϕ = flow coefficient based on compressor inlet condition = $Q/(ND^3)$	φ = head coefficient =H/ u_2^2
η = efficiency	

References

[1] Boyce, M.P, 2003 “Centrifugal compressor: a basic guide,” PennWell Corparation, Tulsa, OK, USA.
[2] Japikse, D., 1996, “Centrifugal compressor design and performance,” Concepts ETI, VT, USA.
[3] Zangeneh, M., Vogt, D. and Roduner, C., 2002, “Improving a vaned diffuser for a given centrifugal impeller by 3D inverse design,” Presented at the ASME TURBO EXPO 2002, Amsterdam, Netherlands, June 3-6 2002. ASME paper no. GT-2002-30621.
[4] Amineni, N. K., and Engeda, A., 1997, “Pressure recovery in low solidity vaned diffusers for centrifugal compressors,” 97-GT-472.
[5] Senoo, Y., Hayami, H. and Ueki, H., 1983, “Low solidity trandem cascade diffusers for wide flow range centrifugal blowers,” 83-GT-3.
[6] Xu, C, Amano, R. S. and E. K. Lee, 2004, “ Investigation of an axial fan—Blade stress and vibration due to aerodynamic pressure field and centrifugal effects,” JSME International Journal, series b, vol. 47, No. 1, pp. 75-90.
[7] Kenny, D. P. 1984, “The history and future of the centrifugal compressor in aviation gas turbine,” 1st Cliff Garrett Turbomachinery Award Lecture, Society of Automotive Engineers, SAE/SP-804/602.
[8] Xu, C. and Amano, R.S., 2009, “On the Development of Turbomachine Blade Aerodynamic Design System,” International Journal for Computational Methods in Engineering Science & Mechanics Vol. 10, Issue 3, pp. 186-196.
[9] Xu, C and Amano, R. S., 2002, “Turbomachinery Blade Aerodynamic Design and Optimization,” GT-2002-30541, 2002.
[10] Weber C R, and Koronowski, M E, 1987, “Meanline performance prediction of volutes in Centrifugal compressors,” ASME 31st Gas Turbine Conference and Exhibit, Dusseldorf, Germany, 86-GT-216.
[11] Dong, R., Chu, S., and Katz, J., 1997, “Effect of Modification to Tongue and impeller Geometry on Unsteady Flow, Pressure Fluctuations and Noise in a Centrifugal Pump,” ASME J. Turbomach., 119, PP. 506-515.
[12] Arora, J.S., 1998, Introduction to Optimum Design, NY, MC Graw-Hill.
[13] D. Bonaiuti, A. Arnone, M. Ermini, and L. Baldassarre, “Analysis and Optimization of transonic centrifugal Compressor Impellers Using the Design of Experiments Technique,” G T-2002-30619.
[14] Xu, C. and Amano, R.S., “A Hybrid Numerical Procedure for Cascade Flow Analysis,” Numerical Heat Transfer, Part B, 2000, Vol. 37, No. 2, pp. 141-164.
[15] Xu, C. and Amano, R.S., “Computational Analysis of Pitch-Width Effects on the Secondary Flows Of Turbine Blades,” Computational Mechanics, Vol. 34, No. 2, 2004, pp. 111-120.
[16] Harry, M. J., 1997, “The nature of Six Sigma quality,” Motorola Univ. Press., Shaumburg, Illinois.
[17] Xu, C. and Valentine D, 1997, “Diffuser for a centrifugal compressor,” US patent # 7581925.
[18] CFX Ltd, 2003, “CFX5, version 5.6,” UK.
[19] ASME, Performance Test Code on Compressors and Exhausters, PTC 10-97, 1997.